Microchemical Journal 96 (2010) 259–268

Contents lists available at ScienceDirect

Microchemical Journal

journal homepage: www.elsevier.com/locate/microc

X-ray and scanning electron microscopy archaeometric studies of pigments from the Aguada culture, Argentina

V. Galván Josa [a], S.R. Bertolino [a,b], A. Laguens [b,c], J.A. Riveros [a,b], G. Castellano [a,b,*]

[a] FaMAF, Universidad Nacional de Córdoba, Medina Allende s/n, Ciudad Universitaria, (5016) Córdoba, Argentina
[b] CONICET, Argentina
[c] Museo de Antropología, FFyH, Universidad Nacional de Córdoba. H. Irigoyen 174, (5000) Córdoba, Argentina

ARTICLE INFO

Article history:
Received 27 February 2010
Received in revised form 23 March 2010
Accepted 23 March 2010
Available online 30 March 2010

Keywords:
SEM
EDX
XRD
Aguada culture

ABSTRACT

X-ray diffraction (XRD) and scanning electron microscopy (SEM) with energy-dispersive system (EDX) were used in order to obtain mineralogical and chemical composition of white and reddish pigments belonging to the Ambato style of "Aguada" culture, found in the archaeological site of Piedras Blancas (Catamarca, Argentina 500–1100 AD). These pigments are associated with different sectors, two of them being related to funerary context. Due the scarce amount of samples available, it was necessary to develop a new methodology for their study. X-ray diffraction spectra were collected using a low background Si sample holder, which allows the study of small sample amounts (a few milligrams). The mineral quantifications were carried out by applying the Rietveld method to the XRD spectra. The major difficulties arose for reddish pigments, since they contain iron-bearing phases, such as ferruginous clays, in which neither the concentration of Fe^{+2} relative to Fe^{+3} nor the location in the lattice (occupancy factor) is completely known. With the aim of performing quantitative elemental analysis from SEM-EDX spectra, a special sample holder for the small amounts of available samples was developed. Commercial standards were used in the quantification process and the characteristic intensities were corrected for matrix effects. Micrographs and EDX point spectra allowed the characterization of minor phases and particle analysis. The Rietveld method combined with the new procedure for EDX analysis has proven to be a suitable method for routine quantitative analysis of small amounts of archaeological pigments.

1. Introduction

The application of analytical techniques, initially developed in the field of materials science, to study objects of art and archaeology gives the art historians and archaeologists the opportunity of gaining information about the composition of such objects and, therefore, to answer questions regarding where, when or by whom such artifacts were made. Additionally, these investigations can help to understand the manufacturing processes and technology, thus providing clues to interpret the social, political, economic and cultural context of the civilizations studied. Such investigations are also valuable and in some cases indispensable for conservation, restoration and authentication projects [1].

Usually archaeological pigments are not found pure, but mixed with a binder and applied to a surface (pottery, walls, wares, leather, caves, etc.). Laser Ablation-Inductively Coupled Plasma-Mass Spectrometry (LAICP-MS) [2–5] and Neutron Activation Analysis (NAA) [6–9] are techniques also used for chemical characterization, and permit a limit of detection (LOD) of a few parts per billion (ppb = ng/g); however, they present the disadvantage of high-cost analysis and limited availability of nuclear reactor centers in the case of neutron activation [2,5,10]. These disadvantages inhibit a frequent use of these techniques.

X-ray nondestructive analytical techniques such as scanning electron microscopy (SEM) in combination with energy-dispersive spectrometry and X-ray diffraction (XRD) have been widely used for the analysis of archaeological paints [11–19]. Their popularity lies not only in the nondestructive character and relatively low-cost analysis, but also in the fact that their simultaneous application allows a mineralogical (XRD) and chemical (XRF, TXRF and SEM-EDX) characterization of samples [11,18–21].

The analysis of paints and pigments is one of the most interesting aspects, not only in archaeology, but also in the history of art, to understand deterioration processes and to develop conservation methods. As mentioned above, a number of works have been devoted to the characterization of paints (a pigment added to a binder), although little has been done regarding pigments. Archaeological paints may have been elaborated with different natural pigments, and they may contain organic components (bones, fats, etc.) or inorganic ones (minerals). The present work aims to give an important step

* Corresponding author. FaMAF, Universidad Nacional de Córdoba, Medina Allende s/n, Ciudad Universitaria, (5016) Córdoba, Argentina. Tel.: +54 351 4334051; fax: +54 351 4334054.
E-mail address: gcas@famaf.unc.edu.ar (G. Castellano).

0026-265X/$ – see front matter © 2010 Elsevier B.V. All rights reserved.
doi:10.1016/j.microc.2010.03.010

forward in the chemical and mineralogical quantitative characterization of archaeological pigments corresponding to the Ambato style of Aguada culture (Catamarca province, Argentina). According to different studies [22–24], this culture flourished during the IV and XII centuries AD, and an exhaustive study of pigments and paints applied to different objects has not been completed yet, only qualitative analysis being found in the literature [25–27]. The characterization provided in this work will complement previous results in this area [26–29], and may contribute with the elaboration of a database of archaeological pigments composition used in ancient America.

The identification of potential clay sources is a relevant issue in the understanding of exchange mechanisms and technology processes of the cultures involved. Nevertheless, this identification is usually hindered, for example, in the analysis of paints scraped from the surface of archaeological sherds, due to the fact that clay mineral structure changes during the firing process. In this work, however, it is worth emphasizing that in these samples, the mineralogy has not been altered by manufacturing processes.

The methodology proposed in this work begins with the observation of fresh samples through SEM images, and, through backscattered electron (BE) images, small regions of different atomic mean numbers are analyzed. Qualitative compositions are then obtained from EDX point spectra of selected regions. After grinding and compacting of samples, mineral phases are then identified from the XRD spectra and they are quantified by a Rietveld refinement procedure. Finally, SEM-EDX spectra are acquired in order to determine the elemental compositions. This methodology is helpful not only to characterize this kind of pigments, but also to study painted surfaces, even when scraped from artifacts such as ceramic pieces, since in the latter case the amount of material that can be extracted is too small for chemical analysis.

2. Analytical techniques

2.1. Electron probe quantitation

In conventional electron probe quantitation, the characteristic intensity I_j emitted by each element of an unknown sample is recorded and then compared with the corresponding intensity I_j^0 emitted from a standard of concentration C_j^0. As a first approximation, the intensity I_j may be taken as proportional to the mass concentration C_j of element j:

$$\frac{I_j}{I_j^0} = \frac{C_j}{C_j^0}.$$

The comparison with the standard allows to eliminate geometrical and physical factors which are very difficult to determine [30]. The previous relationship has no general validity, and different matrix effects must be taken into account, usually referred to as "*ZAF* correction" [30,31]: *Z* and *A* factors represent the generation, scattering and absorption effects, whereas the *F* factor involves secondary fluorescence enhancement; since these effects may differ from sample to standard, the *ZAF* correction is necessary in order to accurately relate the sample composition with the measured characteristic intensities. The magnitude of the *Z*, *A*, and *F* correction factors strongly depends on the experimental conditions, mainly on the incident beam energy, X-ray take-off angle and differences in composition of the standards used as compared to the unknown samples. In some cases, it is possible to reduce their influence and even compensate effects, provided the experimental conditions are adequately chosen.

Matrix effects involve all elements in the sample, with a complex functional dependence on the concentrations. In the program MULTI [32] used in this work, an iterative method is implemented for assessing the complete set of concentrations C_j. This algorithm allows the quantification of an unknown sample with up to eighteen elements, which can be compared to several standards in any kind of combinations, ranging from one standard containing all the analytes to one standard for each analyte. Moreover, it is possible to perform analysis of light elements if stoichiometric relationships are known. In addition, several *ZAF* correction models may be selected, from which the Gaussian model for the *ZA* correction [33] modified by Riveros et al. [34] along with Reed's fluorescence correction factor *F* [35] were chosen for the present analysis.

It is very important to take into account the different issues which may alter the X-ray spectrum acquired, and therefore distort the quantitative results obtained. If the sample is an insulator or the conductive coating is inadequate, surface charging effects can create a noticeable modification of the X-ray emission spectra, and the results of the quantifications will be incorrect. A strategy which permits to account for charging effects is to determine the Duane–Hunt limit, which represents the maximum energy of the continuum X-ray spectrum produced by the incident beam impacting on the sample surface [36]. The conventional method to evaluate the Duane–Hunt limit value is to (linearly) fit the region before the cut-off energy. The energy values obtained this way were used as input for the quantification procedure with the program MULTI [32].

2.2. XRD Rietveld refinement

The Rietveld refinement method uses a least squares approach to refine a theoretical XRD spectrum until it matches the measured profile [37]. The model for the calculated profile includes structural (spatial groups, atoms in the asymmetric units, thermic factors, etc.), microstructural (concentration, crystal size, micro deformations), and instrumental (full width at half maximum, width of slits, size of the sample, depth of X-ray penetration, etc.) factors.

A Pearson VII profile function [38] was used in this work for approximating the X-ray diffraction peaks; this model, based on a Gaussian function multiplied by a correction factor in the form of a series expansion in Hermite polynomials, was chosen since it takes into account the asymmetry of the peaks. The preferred orientation effects were corrected for the easily orientable phases (e.g. phyllosilicates and feldspars). The background was fitted using a sixth degree polynomial function. Parameters related to thermal fluctuations were not refined, since their influence will be negligible as compared to the uncertainties introduced by the refinement of occupancy factors, in view of the poor statistics associated to the minor phases. The values for these parameters were taken from the Inorganic Crystal Structure Database (ICSD)[1] indexed files corresponding to each mineral.

In order to provide a figure of merit for the performance of each fit, the goodness of fit is assessed through the weighted comparison of the predicted intensities $\tilde{Y}_i$ with the experimental ones Y_i:

$$GOF = \sqrt{\frac{1}{N-P}\sum_{i=1}^{N}\frac{\left(Y_i-\tilde{Y}_i\right)^2}{Y_i}}$$

where i denotes each of the N channels in the considered XRD spectrum, and P is the number of free parameters in the fitting process [37]. The statistical quality of the fit is represented through the R_e parameter, defined as

$$R_e = \sqrt{\frac{N-P}{\sum Y_i}}.$$

[1] http://icsd.fiz-karlsruhe.de/icsd.

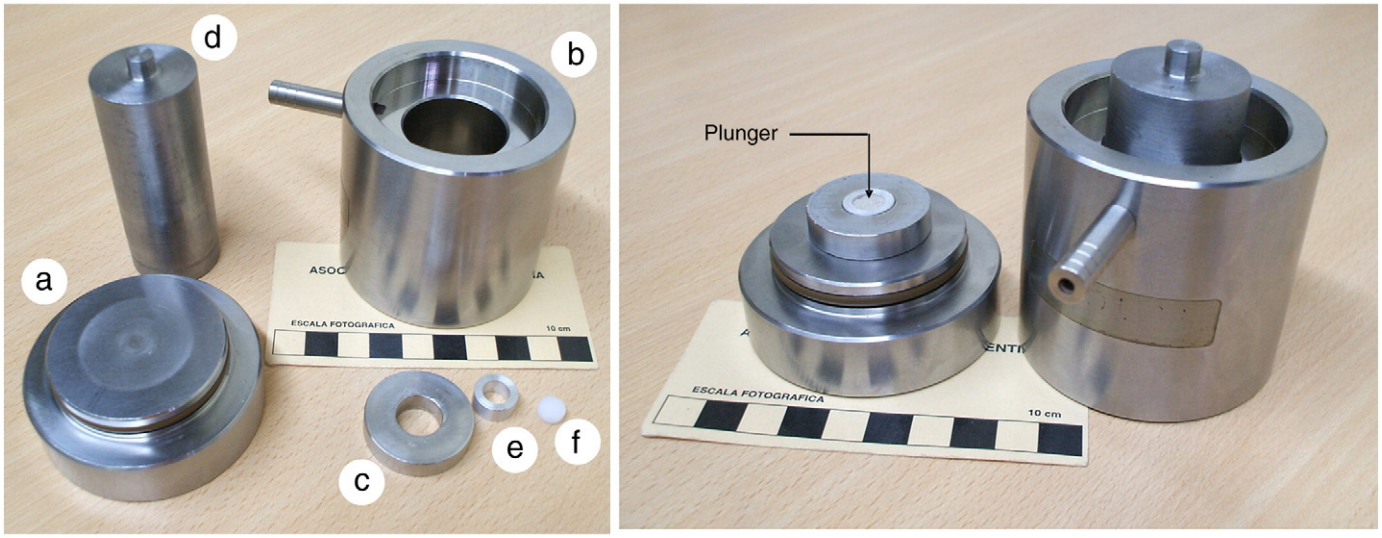

Fig. 1. Sample holder designed for pigment analysis through EDX spectrum acquisition. a) Supporting base, b) skirt, c) container ring, d) piston, e) sample supporting ring, and f) plunger.

3. Materials

Samples consisted of aggregates of very fine particles taken from different locations at the archaeological site of Piedras Blancas, only a few tens of milligrams being available for analysis. The analyzed samples have been labeled according to the following scheme: W1, W2, W3, W4, W5, W6 and W7 correspond to white pigments, whereas R1, R2, R3 and R4 are reddish pigments. Samples W2 and R1 were found in a funerary context, whereas the others were found associated with domestic and working sectors.

4. Experimental

4.1. Sample preparation

For a quantitative analysis by SEM-EDX, the samples should be flat and the electron beam must impact normal to the surface. To achieve this purpose, all samples were ground and compacted into a sample holder specially developed to this aim. The compaction was performed by applying a pressure of 20 t/cm^2 during 20 min, by means of a Teflon plunger located between piston and sample. After compaction, this plunger remains attached to the aluminium cylinder as a sample support, thus ensuring a homogeneous density. By this procedure, a small amount of sample (10 mg) is compacted covering an area of 0.5 cm^2, allowing several analyses in different regions of it. In Fig. 1 the main components of the sample holder designed are shown.

To acquire EDX spectra, the samples were not coated, due to the fact that, on one hand, carbon coating complicates the quantification of these elements, and on the other hand the presence of a gold coating (or other heavy metal layer) modifies the different absorption effects for each line, and implies the appearance of its characteristic peaks, which may overlap with some lines of interest. This is the case of gold M lines overlapping with sulfur K and lead M lines.

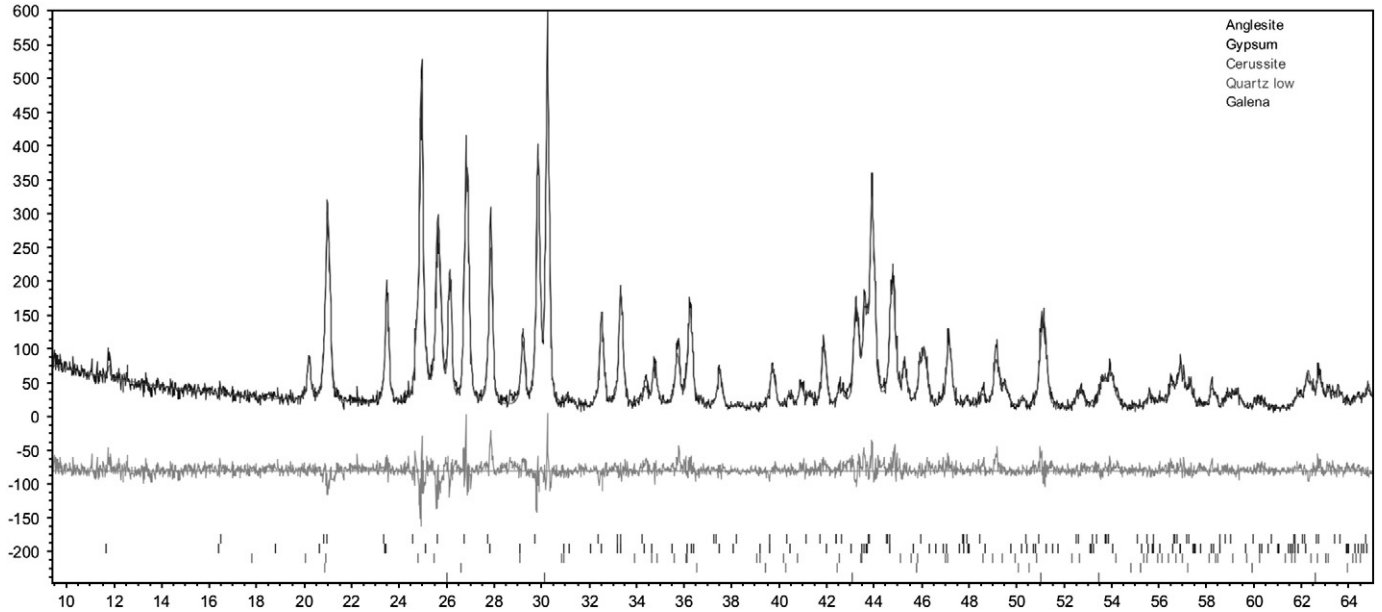

Fig. 2. Rietveld refinement for the W2 XRD spectrum. The upper curves are the measured and calculated spectra respectively. The lower curve shows the difference between observed and calculated patterns.

Table 1
Mineralogical quantification obtained with XRD.

Phase concentrations (wt.%)												
Mineral	ICSD code	Structure	White							Reddish			
			W1	W2	W3	W4	W5	W6	W7	R1	R2	R3	R4
Calcite	80869	$CaCO_3$	96.0		96.7	57.8	100		71.4		5.9		
Quartz	174	SiO_2	4.0	8.8	1.7	3.3			12.0	19.0	41.7	13.4	32
Albite	34917	$NaAlSi_3O_8$			1.6					33.3	17.6		54.1
Hematite	56372	Fe_2O_3							3.8	2.7	11.7	58.7	2.3
Muscovite	4368	$KAl_2(AlSi_3O_{10})(OH)_2$				7				45.0		3.7	11.6
Gypsum	409581	H_4CaO_6S		3.3				100			24.2		
Feldespar	88896	K (Al Si_3O_8)							12.4				
Anorthite	86331	Ca (Al2 Si2 O8)				31.9							
Litharge	15466	PbO							0.4				
Anlgesite	100625	$PbSO_4$		49.7									
Cerussite	36554	$PbCO_3$		27.7									
Galena	38293	PbS		10.5									
Tourmaline	156163	$NaFe_3Al_6Si_6O_18(BO_3)_3O_3F$										24.2	
Kaolinite	63192	$Al_2(Si_2O_5(OH)_4)$									3.9		
R_{wp} (%)			12.42	16.8	14.55	15.86			16.31	18.59	22.98	21.72	18.67
R_e (%)			9.54	13.71	11.65	10.32			9.52	12.34	13.47	9.78	7.50
GOF			1.30	1.23	1.25	1.53			1.71	1.51	1.71	2.22	2.49

4.2. SEM images

Previous to the acquisition of EDX and XRD spectra, secondary electron (SE) images of nonmilled samples were registered in order to analyze the particle size distribution and microstructure, and to corroborate the occurrence of the presence of minor phases whose species are not easily identifiable by XRD.

Backscattered electron (BE) images were taken to distinguish regions with noticeable chemical-contrast differences, since backscattered electrons allow the distinction of small variations in the mean atomic number [31], which might help to identify different phases. With the aid of EDX spectra taken from points with high magnification, a qualitative compositional estimate of small particles may be given, complementing the information provided by the BE images acquired. Although these spectra are not representative of the overall sample, the identification of particles (or phases) present in very low proportion may be useful for the study of the provenance of raw materials.

4.3. XRD measurements

Samples prepared in random mounts were analyzed on a Philips X'Pert PRO PW3040/60 diffractometer, with Cu Kα X-ray radiation, Si monochromator, at 40 kV and 30 mA, step scan at 0.3°/min and step size of 0.02° 2θ. In most cases, since too small amounts (a few milligrams) of material were available, samples were mounted on an Si holder of low background.

The mineral phases present were quantified by Rietveld refinement, as implemented in the DiffracPlus TOPAS® commercial software. The LOD of this technique for the samples studied is estimated

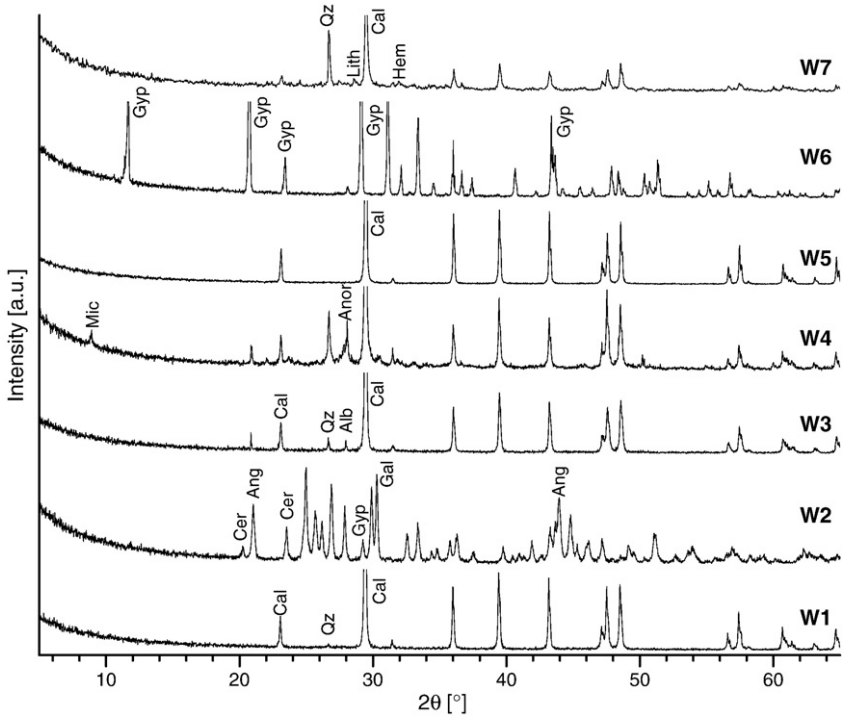

Fig. 3. XRD patterns corresponding to the white pigments. The identified phases are also shown in the figure. Alb: Albite; Ang: anglesite; Anor: Anorthite; Cer: Cerussite; Gal: Galena; Gyp: Gypsum; Hem: Hematite; Lith: Litharge; Mic: Mica; Ort: Orthoclase; and Qz: Quartz.

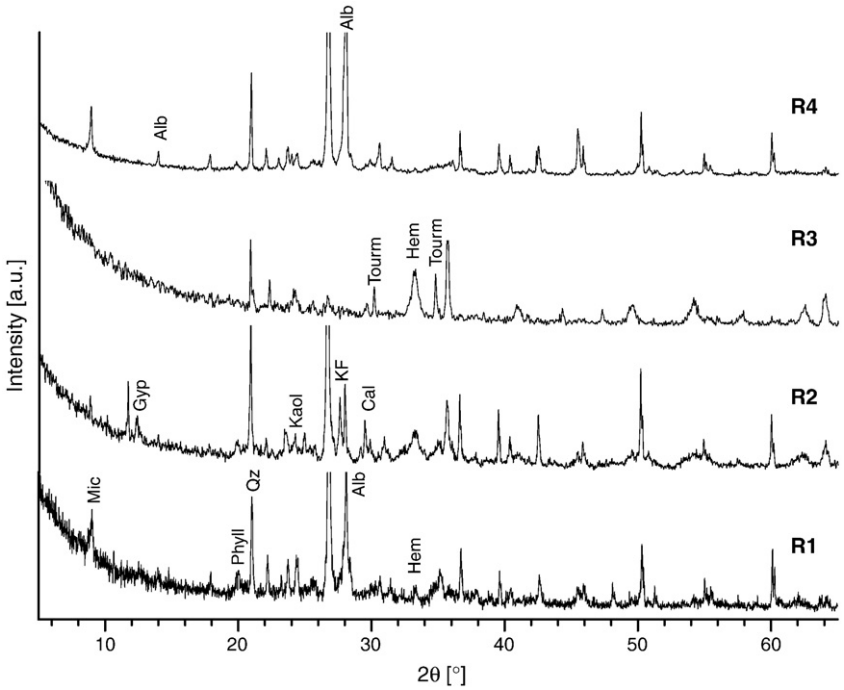

Fig. 4. XRD patterns corresponding to the reddish pigments. The identified phases are also shown in the figure. Alb: Albite; Ang: Anglesite; Cal: Calcite; Cer: Cerussite; Gal: Galena; Gyp: Gypsum; Hem: Hematite; Kaol: Kaolinite; Mic: Mica; KF: Potassium feldspar; Phy: Phyllosilicates; Qz: Quartz; and Tourm: Tourmaline.

between 1 and 2%. Fig. 2 shows an example of the fit quality achieved in the refinement process for the sample W2.

4.4. EDX spectra

In order to obtain chemical compositions, a scanning electron microscope LEO 1450 VP with an energy-dispersive spectrometer attached was used. The Sapphire Ultra-Thin Window X-ray detector allows the detection of elements with atomic number greater than 5, with a resolution of 129.2 eV for the Mn-Kα line.

In all cases, the acquisition live time was 200 s, nominal incident beam energy $E_o = 15$ keV, 500 pA specimen current, 15 mm working distance and 33.42° take-off angle. In order to obtain a representative analysis of each sample, the probe current was checked at the beginning and at the end of each measurement with a Faraday cup;

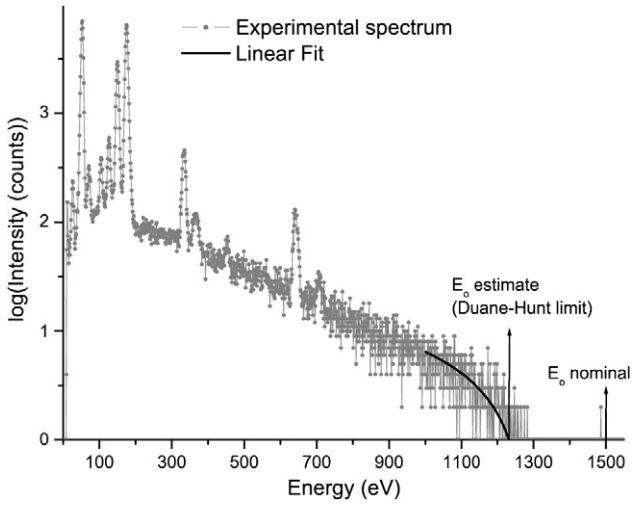

Fig. 5. Determination of the effective incident energy value for R1 sample from the Duane–Hunt limit.

Table 2
Elemental concentrations of white pigments obtained with SEM-EDX analysis.

Elemental concentrations (wt.%)							
Sample	W1	W2	W3	W4	W5	W6	W7
E_0^* (keV)	14.6	14.6	15.0	14.0	14.8	14.8	13.1
Element							
C	11.4[a]	1.2[a]	10.9[a]	10.0[a]	13.9[a]		9.9[a]
O	47.6[a]	20.6[a]	46.3[a]	51.3[a]	43.7[a]	60.9[a]	44.1[a]
Na		0.7	0.1		0.1		0.3
Mg	0.2		0.5	1.5	0.2		1.7
Al	0.3	0.9	0.4	2.4	0.4		1.8
Si	1.0	4.9	1.7	8.0	1.1		8.5
P			0.1				0.1
S		5.8	0.8			17.7	
K	0.3	0.6	0.5	1.5	0.4		3.8
Ca	38.2	1.6	36.1	23.1	37.2	21.3	26.6
Mn		1.0					
Fe	0.2	2.3	0.3	1.7	0.26		1.8
Pb		63.2[b]					

[a] Assessed by stoichiometry.
[b] Calculated through Mα-line intensities.

Table 3
Elemental concentrations of reddish pigments obtained with SEM-EDX analysis.

Elemental concentrations (wt.%)				
Sample	R1	R2	R3	R4
E_0^* (keV)	12.3	13.7	13.5	12.9
Element				
C	2.9	0.7[a]		
O	50.4[a]	44.3[a]	43[a]	44.1[a]
Na	1.1	0.6	0.4	5.0
Mg	1.7	0.8	0.6	0.8
Al	9.0	6.6	7	7.4
Si	23.8	21	22.8	27.7
S		2.7		
K	7	5	5.2	7.3
Ca	0.5	2	2	1.1
Fe	4.6	17.4	19	4.1

[a] Assessed by stoichiometry.

Table 4
Mass concentrations obtained for sample R1 using the nominal incident energy (15 keV) and that determined through the Duane–Hunt limit (12.3 keV).

R1 sample (wt.%)		
Element	$E_0{}^* = 15.0$ keV	$E_0{}^* = 12.3$ keV
C	3.06[a]	2.87
O	46.02[a]	50.41
Na	1.02	1.14
Mg	1.37	1.69
Al	7.12	9.03
Si	18.22	23.78
K	4.47	6.63
Ca	0.31	0.5
Ti	0.24	0.43
Fe	2.31	4.62
Total	84.16	101.1

[a] Assessed by stoichiometry.

this allowed to verify that probe current variations remained within 1%.

5. Results and discussion

5.1. XRD

In the Rietveld refinement procedure, the effects induced by the preferred orientation inherent to the sample preparation method were considered. The major difficulties in the refinement process occur for the reddish pigments, because of the presence of iron-bearing phases such as ferruginous clays for which neither the concentration of the Fe^{+2} with respect to Fe^{+3}, nor their localization in the lattice (occupation factor) are known. In addition, in some cases the major phase peaks are overlapped with the principal lines of minor phases, hindering the deconvolution process and raising the LOD up to about 3%. The *R* factors [37] (numerical criteria of fit) obtained from the refinement results are listed in Table 1. The apparently high values for R_e (and hence for R_{wp})

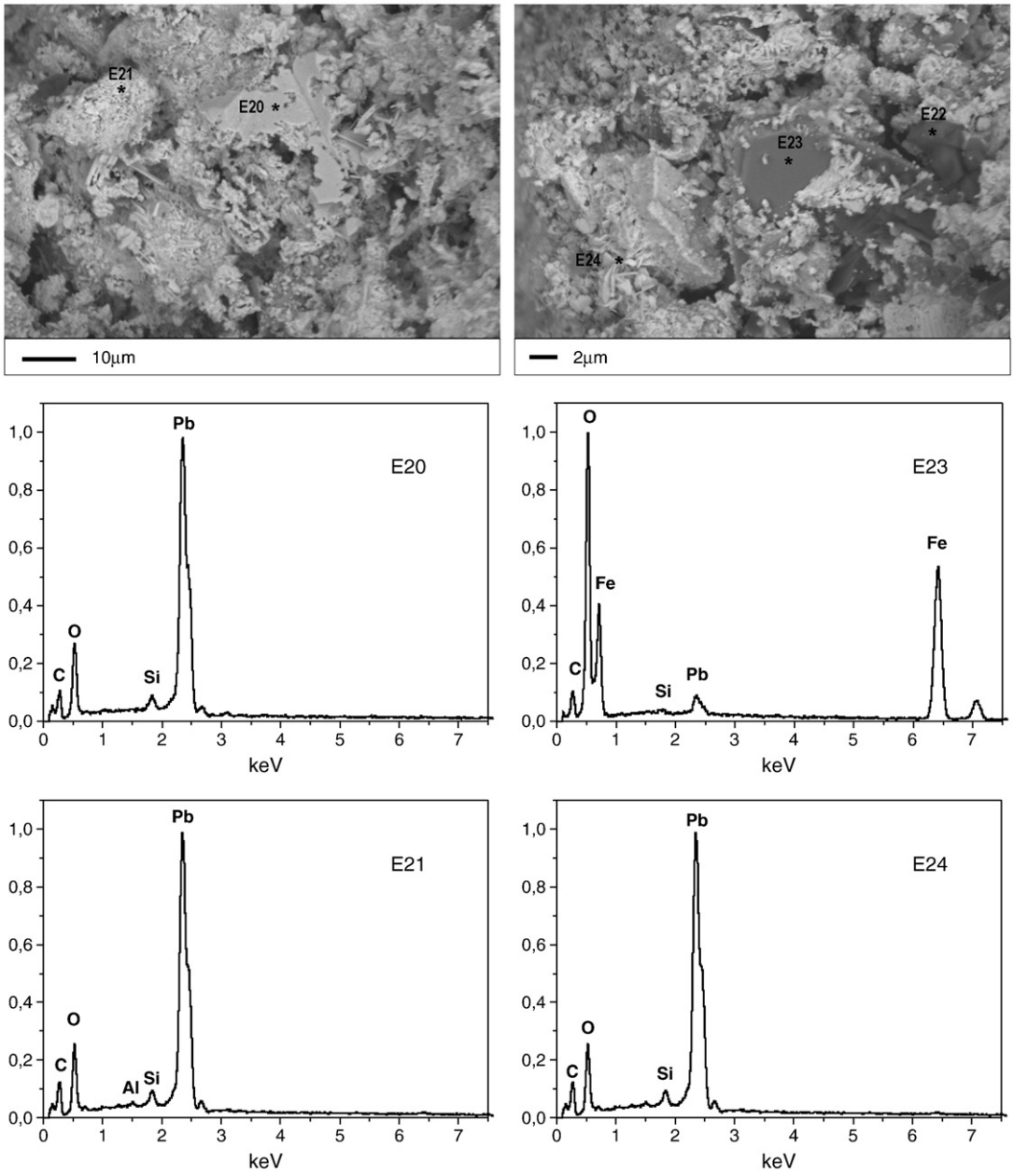

Fig. 6. BE images and X-ray spectra corresponding to the indicated points for the W2 sample.

evidence the difficulties mentioned above for the characterization of reddish pigments. Nevertheless, although the values obtained for R_{wp} seem to be too large, it must be pointed out that since a rather small amount of material is to be analyzed, statistics cannot be noticeably improved due to the unavoidable experimental limitations this implies.

As shown in Table 1 and Fig. 3, white pigments W1, W3 and W5 are characterized by the content of more than 90% of calcite. This suggests that this mineral could be the colour source. The W6 pigment is pure gypsum, whereas the pigments W4 and W7 contain, besides calcite (in a concentration lesser than 50%), quartz, micas and feldspars. These phases act as an embedding flux and could result in a glassy finish if the pigment is applied on the ceramic pot before cooking.

The W2 sample found in the mortuary context presents a very different mineralogical composition. It contains a high concentration of lead distributed in anglesite, cerussite and galena phases. Lead is also present in the pigment W7, which is an example where the characteristic colour is due to minor phases: it is well known that even small proportions of lead mixed in a translucent medium (e.g. quartz) result in a good white pigment [28]. The characteristic diffraction peaks corresponding to these phases can be seen in Fig. 2.

Regarding the reddish pigments, as displayed in Table 1 and Fig. 4, iron oxides are present mainly as hematite, in mixtures with different clays. The pigments R1 and R4 contain similar concentrations of hematite (2–3%), whereas R2 has a higher percentage of hematite (11%), and also contains calcite and gypsum. Finally, the R3 sample contains tourmaline (20%) and high amounts of hematite (56%).

5.2. SEM-EDX

The irradiation parameters used for the acquisition of spectra ensure a LOD of 500 ppm to 1000 ppm, and small matrix effect corrections for most of the elements present in the samples studied. These considerations allow to quantify the major and minor elements with acceptable uncertainties.

As mentioned above, the Duane–Hunt limit value was fitted in order to determine the effective incident beam energies E_0^* which were used as input for the quantification routine by means of the program MULTI [32]. An example of such fitting procedure is shown in Fig. 5 for the reddish pigment R1. The fitted values for the effective incident beam energies corresponding to all the samples analyzed are displayed in Tables 2 and 3. It can be seen that this correction may become quite important (up to 20%).

The influence of the value taken for E_o on the concentrations obtained is exemplified in Table 4 for the R1 sample. Clearly, the dependence of the ZAF matrix corrections on the incident energy is not equal for all elements, since relative concentrations may be strongly altered even for similar E_o values.

The quantification routines were assessed with the software MULTI [32], using SPI® commercial mineral standards. The global uncertainties, associated to the ZAF corrections and to the determination of characteristic intensities, are much lower than the errors due to charging effects and sample preparation.

Table 2 shows the results obtained for the quantification of white pigments through the X-ray characteristic spectra. Excepting for sample W2, white pigments are characterized by a high calcium concentration (between 23% and 38%), which is in agreement with the elemental composition inferred from the mineralogical quantification. Some minor elements (e.g. Na or K) found in W3, W4 and W7 may be associated to feldspar phases. The W2 pigment, found in a funerary context, presents a very different elemental composition with respect to the other pigments studied: the major element is lead, calcium and sulphur being part of the gypsum quantified by Rietveld refinement.

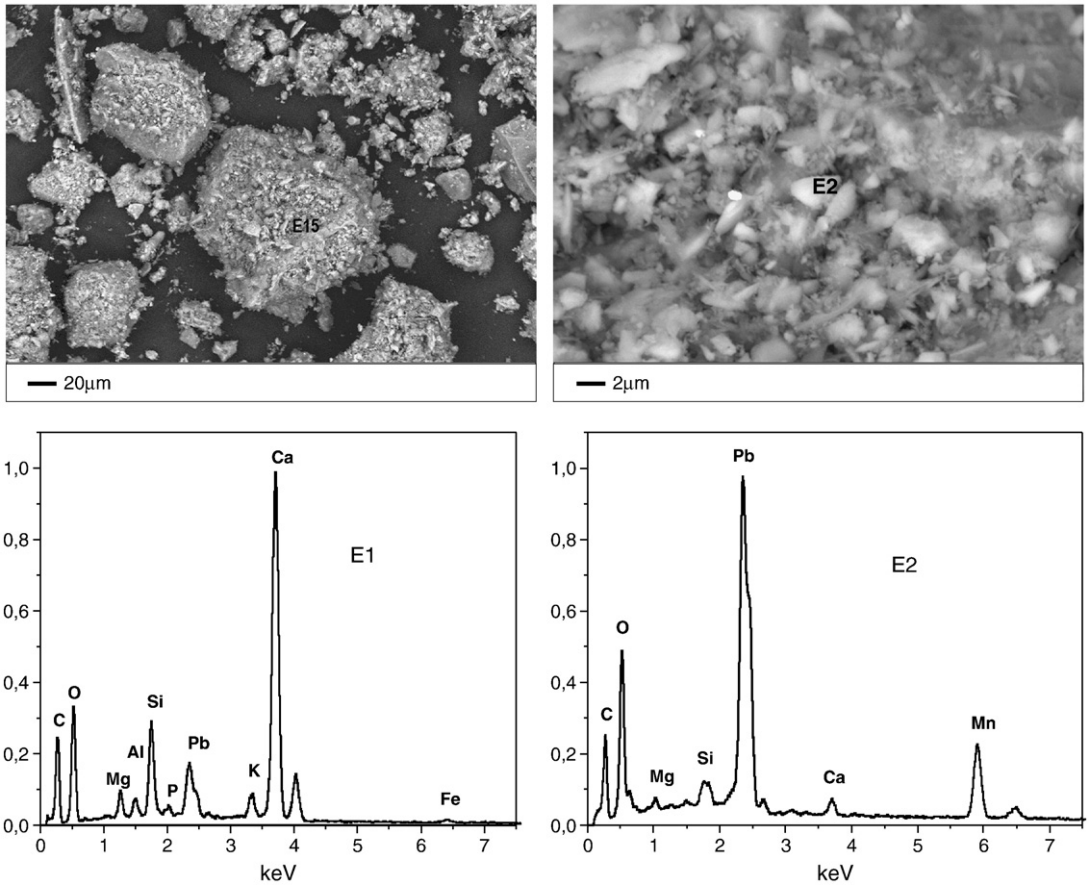

Fig. 7. BE images and X-ray spectra for the indicated points corresponding to the W7 sample.

The correct deconvolution of the spectra in the low energy region is very important because the detector cannot separate the Pb-M lines from S-Kα line. However, the quantification of lead was performed by taking into account the Pb-Mα line, since it is much more intense than the Pb-L lines for the electron beam energy chosen. To this aim, the EDX spectral processing was performed by taking into account radiative transition rates given by Perkins et al. [39].

In Table 3 the elemental composition of red pigments is shown. Samples R1 and R4 have similar compositions, nevertheless small differences in the Ca concentration can be seen. The Fe contents in both samples are consistent with the hematite phase obtained by XRD. According to the results obtained by SEM and XRD, the R2 sample bears a high Fe mass fraction (15.3%), and its Ca content is related to the presence of phases such as calcite, gypsum and albite. Finally, the R3 pigment presents the highest Fe concentration (41%), which is consistent with the amount of hematite and tourmaline detected by XRD.

In both sets of samples, EDX analyses provide compositions similar to those inferred through the XRD refinement procedure. In the case of reddish pigments, some discrepancies arise. It must be mentioned, however, that a wide variety of minerals bear similar crystallographic structures, but a number of ion substitutions may occur, which implies important differences from the 'stoichiometric' formulas chosen for the phase quantification through XRD. In addition, XRD results are overestimated, which is inherent to the phase concentration normalization accomplished by the Rietveld refinement method. Finally, a less important uncertainty is introduced by minor phases present in the sample which cannot be quantified by XRD and may add up to 3%.

The SEM images can be helpful to infer about previous treatments. For example in Figs. 6 and 7, BE images corresponding to the samples W2 and W7 evidence some rod-shaped structures with calcium, but this structures are not calcite, since in the EDX point spectra the carbon intensities are too low. Although these phases could not be

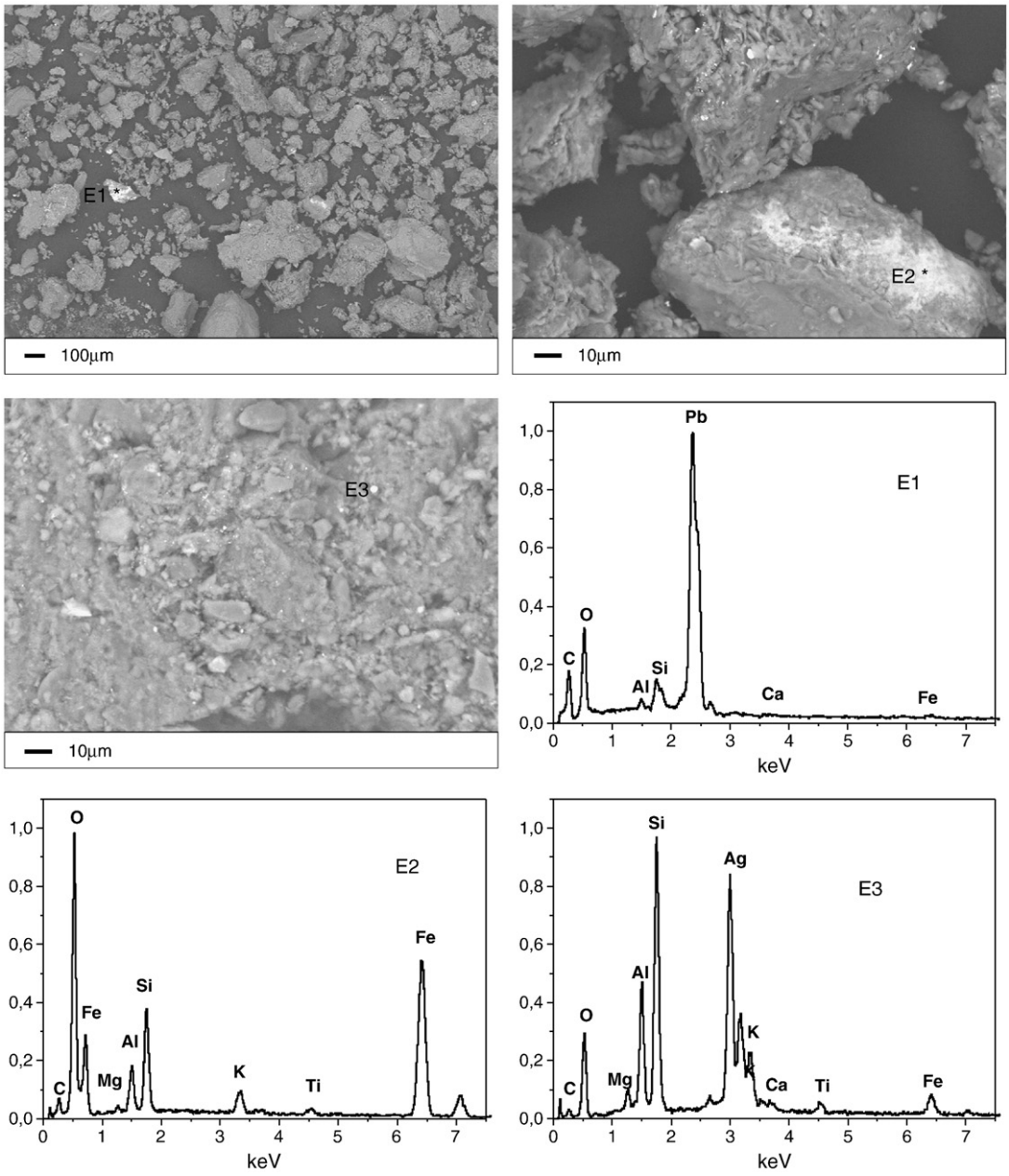

Fig. 8. BE images and X-ray spectra for the indicated points corresponding to the R1 sample.

identified by XRD since they are below the LOD associated to this technique, it is well known that when calcite is fired, CaO and CO_2 are produced, which could be an indication that these pigments were previously cooked [28]. It is worth mentioning that the apparent defocalization of the W7 image may be due to the presence of organic materials as supporting medium for this pigment, such as grease, commonly used as a binder in ancient wall paints.

In the BE images corresponding to the W1, W3, W7 white pigments and the R1 reddish sample, some bright particles can be observed. Since the backscattered electron signal increases with the mean atomic number *Z* of the irradiated sample [30], this chemical contrast is associated with the presence of small particles (about 2 μm diameter) containing Pb (see Figs. 7 and 8). In the R1 sample, particles of Ag (spectrum E1 of Fig. 8) can also be seen. These elements cannot be detected through the EDX global spectrum or the XRD patterns, due to the fact that their concentration is smaller than the LOD (<0.1%).

6. Conclusions

The strengths and weaknesses of the nondestructive techniques SEM-EDX and XRD have been discussed when applied to the characterization of archaeological pigments. By adequately applying both techniques, the chemical and mineralogical compositions of Aguada archaeological pigments were satisfactorily obtained.

The results of the XRD quantifications through Rietveld refinement are normalized to 100% and the LOD attainable from the diffractograms is above 2%. These analyses showed that the pigments W1, W3 and W5 mainly contain calcite, whereas the W6 pigment is pure gypsum and R3 has a major content of hematite, tourmaline and quartz. These pigments can be interpreted as raw material without complex elaboration, whereas samples W2, W4, W7, and the other reddish pigments present a very different mineralogical composition.

With the aim of complementing the results obtained through XRD, SEM-EDX quantifications were performed. To this purpose, surface charge accumulation effects were taken into account by determining the Duane–Hunt limit in order to assess the effective incident energy, which allowed a remarkable improvement of the sets of concentrations obtained. The LODs of the EDX analyses are around 0.1%, allowing to identify minor elements in the phases detected and even the presence of phases not detected by XRD. In both sets of samples, EDX results are consistent with those obtained through the XRD refinement procedure. The advantage of these techniques, when compared with other analytical methods, is the small amount of sample required and the low cost per analysis. The methodology proposed here can be performed routinely in samples of similar characteristics, without the requirement of high X-ray intensity sources, as is the case of a synchrotron facility.

With the aid of BE images, the presence of heavy metals (Pb and Ag) was found in samples W1 and R1. The presence of these minor phases can help to obtain clues about raw material sources and may help to analyze circulation of goods and technology processes in this culture.

The data obtained will also enable to progress in the identification of the potential uses for which these pigments were made (ceramics, walls, rituals, etc.). All these advances will help to develop a database in order to facilitate the restoration work and the certification of authenticity of different parts.

Acknowledgements

This work was financially supported by the FONCYT Agency (project PICT no. 07-17346) to whom the authors are gratefully acknowledged. They are also thankful to Francisco Pasarelli from the Museo de Antropología (UNC) for providing samples.

References

[1] M. Schreiner, B. Frühmann, D. Jembrih-Simbürger, R. Linke, X-rays in art and archaeology — an overview, Adv. X-ray Anal. 47 (2004) 1–17.
[2] D.N. Papadopoulou, G.A. Zachariadis, A.N. Anthemidis, N.C. Tsirliganis, J.A. Stratis, Comparison of a portable micro-X-ray fluorescence spectrometry with inductively coupled plasma atomic emission spectrometry for the ancient ceramics analysis, Spectrochim. Acta Part. B 59 (2004) 1877–1884.
[3] L. Bao-Ping, Z. Jian-Xin, A. Greig, K.D. Collerson, Z. Zhen-Xi, F. Yue-Xin, Potential of Sr isotopic analysis in ceramic provenance studies: characterisation of Chinese stonewares, Nucl. Instr. Meth. Phys. Res. B 240 (2005) 726–732.
[4] E. Cochrane, H. Neff, Investigating compositional diversity among Fijian ceramics with laser ablation-inductively coupled plasma-mass spectrometry (LA-ICP-MS): implications for interaction studies on geologically similar islands, J. Archaeol. Sci. 33 (2006) 378–390.
[5] J. Pérez-Arantegui, M. Resano, E. García-Ruiz, F. Vanhaecke, C. Roldán, J. Ferrero, J. Coll, Characterization of cobalt pigments found in traditional Valencian ceramics by means of laser ablation-inductively coupled plasma mass spectrometry and portable X-ray fluorescence spectrometry, Talanta 74 (2008) 1271–1280.
[6] D. Ben-Shlomo, A. Maeir, H. Mommsen, Neutron activation and petrographic analysis of selected Late Bronze and Iron Age pottery from Tell es-Safi/Gath, Israel, J. Arch. Sci. 35 (2002) 956–964.
[7] R.J. Speakman, E. Stone, M. Glascock, A. Cilingiroglu, P. Zimansky, H. Neff, Neutron activation analysis of Urartian pottery from eastern Anatolia, J. Radioanal. Nucl. Chem. 262 (2004) 119–127.
[8] K.J. Vaughn, C.A. Conlee, H. Neff, K. Schreiber, Ceramic production in ancient Nasca: provenance analysis of pottery from the Early Nasca and Tiza cultures through INAA, J. Archaeol. Sci. 33 (2006) 681–689.
[9] J.H. Moon, S.H. Kim, Y.S. Chung, Y.N. Lee, H.J. Kim, Y.E. Kim YE, Determination of the elemental contents in stream sediments collected from Cheongju city by instrumental neutron activation analysis, Anal. Chim. Acta 619 (2008) 137–142.
[10] H. Odell, Lithic Analysis, 3rd ed.Springer, New York, 2006.
[11] J. Buxeda i Garrigós, Alteration and contamination of archaeological ceramics: the perturbation problem, J. Archaeol. Sci. 26 (1999) 295–313.
[12] E. Aloupi, A.G. Karydas, T. Paradellis, Pigment analysis of wall paintings and ceramics from Greece and Cyprus. The optimum use of X-ray spectrometry on specific archaeological issues, X-Ray Spectrom. 29 (2000) 18–24.
[13] P. Mirti, X-ray microanalysis discloses the secrets of ancient Greek and Roman potters, X-Ray Spectrom. 29 (2000) 63–72.
[14] F. Cariati, P. Fermo, S. Gilardoni, S. Galli, M. Milazzo, A new approach for archaeological ceramics analysis using total reflection X-ray fluorescence spectrometry, Spectrochim. Acta Part B 58 (2003) 177–184.
[15] R. Fernández-Ruiz, M. García-Heras, Study of archaelogical ceramics by total-reflection X-ray fluorescence spectrometry: semi-quantitative approach, Spectrochim. Acta Part. B 62 (2007) 1123–1129.
[16] C. Fortina, I. Memmi Turbanti, F. Grassi, Glazed ceramic manufacturing in Southern Tuscany (Italy): evidence of technological continuity throughout the medieval period (10th–14th centuries), Archaeometry 50 (2008) 30–47.
[17] L. Schleicher, J. Miller, S. Watkins-Kenney, L. Carnes-McNaughton, M. Wilde-Ramsing, Non-destructive chemical characterization of ceramic sherds from Shipwreck 31CR314 and Brunswick Town, North Carolina, Archaeol. Sci. 35 (2008) 2824–2838.
[18] J. Barrios Neira, L. Montealegre, L. López, L. Romero, Ceramics of Ategua (Córdoba, Spain): mineralogical and petrographic study, Appl. Clay Sci. 42 (2009) 529–537.
[19] A. Iordanidis, J. Garcia-Guines, G. Karamitrou-Mentessidi, Analytical study of ancient pottery from the archaelogical site of Aiani, northern Greece, Mater. Charact. 60 (2009) 292–302.
[20] C.R. Appolonia, F.R. Espinoza Quiñones, P.H.A. Aragão, A.O. dos Santos, L.M. da Silva, P.F. Barbieri, V.F. do Nascimento Filho, M.M. Coimbra, EDXRF study of Tupi-Guarani archaeological ceramics, Radiat. Phys. Chem. 61 (2001) 711–712.
[21] N. Craig, R. Speakman, R. Popelka-Filcoff, M. Glascock, J. Robertson, M. Aldenderfer Shackley, Comparison of XRF and PXRF for analysis of archaelogical obsidian from southern Perú, J. Archaeol. Sci. 34 (2007) 2012–2024.
[22] M. Baldini, J. Carbonari, G. Cieza, M. de Feo, M. del Castillo, A. Figini, A. Rex González, R. Huarte, J. Togo, Primer análisis de la cronología obtenida en el sitio Choya 68 (Depto. de Capayán, Provincia de Catamarca, Argentina), Estudios Atacameño 24 (2002) 71–82.
[23] A. Laguens, M. Bonnin, Recursos materiales y desigualdad social en la arqueología de Ambato, Catamarca, La Cultura de la Aguada y sus expresiones regionales, EUDELAR, Universidad Nacional de La Rioja, La Rioja, 2005, pp. 23–34.
[24] M. Pantorrilla, V. Núñez Regueiro, Investigaciones arqueológicas en la zona de Escaba, provincia de Tucumán: asentamientos Condorhuasi y Aguada en las Yungas, Intersecciones en Antropología 7 (2006) 235–245.
[25] S.R. Bertolino, M. Fabra, Provenance and ceramic technology of pot sherds from ancient Andean cultures at the Ambato valley, Argentina, Appl. Clay Sci. 24 (2003) 21–34.
[26] G. De La Fuente, N. Kristcautzky, G. Toselli, A. Riveros: Petrología cerámica comparativa y análisis composicional de las pinturas por MEB-EDS de estilo Aguada Portezuelo (ca. 600–900 DC) en el valle de Catamarca (Noroeste Argentino), Estudios Atacameños 30 (2005) 61–78. Available from http://www.scielo.cl/scielo.php?script=sci arttext&pid=S0718-10432005000200004 (in Spanish).
[27] G. De La Fuente, Technological study of pigments and paints on archaeological ceramics from the northwestern Argentine region: an archaeometric approach and implications for conservation, Glass Ceram. Conserv. 14 (2006) 3–6.
[28] S.R. Bertolino, V. Galván, A. Carreras, A. Laguens, G. De La Fuente, A. Riveros, X-ray techniques applied to surface paintings of ceramic pottery pieces from Aguada Culture (Catamarca, Argentina), X-Ray Spectrom. 38 (2009) 95–102.

[29] V. Galván Josa, S.R. Bertolino, J.A. Riveros, G. Castellano, Methodology for processing backscattered electron images, application to Aguada archaeological paints, Micron 40 (2009) 794–799.
[30] S. Reed, Electron Probe Microanalysis, 2nd ed.Cambridge University Press, Cambridge, 1993.
[31] J. Goldstein, D. Newbury, P. Echlin, D. Joy, A. Romig, C. Lyman, C. Fiori, E. Lifshin, Scanning Electron Microscopy and X-ray Microanalysis: A Text for Biologists, Materials Scientists, and Geologists, Plenum Press, New York, 1992.
[32] J. Trincavelli, G. Castellano, J. Riveros, Model for the bremsstrahlung spectrum in EPMA. Application to standardless quantification, X-Ray Spectrom. 27 (1998) 81–86.
[33] R. Packwood, J. Brown, A Gaussian expression to describe φ(ρz) curves for quantitative electron probe microanalysis, X-Ray Spectrom. 10 (1981) 138–145.
[34] J. Riveros, G. Castellano, J. Trincavelli, Comparison of φ(ρz) curves in EPMA, Mikrochim. Acta 12 (Suppl) (1992) 99–105.
[35] S. Reed, Characteristic fluorescence corrections in electron-probe microanalysis, Br. J. Appl Phys 16 (1965) 913–926.
[36] D.E. Newbury, Barriers to quantitative electron probe X-ray microanalysis for low voltage scanning electron microscopy, J. Res. Natl. Inst. Stand. Technol. 107 (2002) 567–603.
[37] R. Young, The Rietveld Method, International Union of Crystallography, Oxford University Press, Oxford, 1993.
[38] S. Enzo, W. Parish, A method of background subtraction for the analysis of broadened profiles, Adv. in X-Ray Anal. 27 (1983) 37–44.
[39] S.T. Perkins, D.E. Cullen, M.H. Chen, J.H. Hubbell, J. Rathkopf, J. Scofield. Tables and graphs of atomic subshells and relaxation data derived from LLNL evaluated atomic data library (EADL), $Z = 1–100$, Lawrence Livermore National Laboratory, Report UCRL-50400, vol. 30 (1991).